Original Paper

Glass and glass-ceramic from basic oxygen furnace (BOF) slag

Eduardo B. Ferreira and Edgar D. Zanotto
LaMaV/DEMa, Federal University of Sao Carlos, SP (Brazil)

Luis A. M. Scudeller
Usiminas Steel Co., Ipatinga, MG (Brazil)

A method is presented to produce glass-ceramics from a BOF slag glass containing a high amount of iron. The composition design of these unusual glasses, their melting and crystallization behavior, their crystal nucleation kinetics and the microstructures resulting from different thermal treatments are analyzed and discussed. Several compositions were tested, varying the proportions of slag, sand and Na_2CO_3 in the batch. A batch with a composition (in wt%) of 60 slag, 35 sand, 5 Na_2O showed good vitrificability and displayed bulk crystallization after thermal treatment, and was therefore chosen for a more detailed study. Crystallized materials with nanometric microstructures were obtained using suitable treatments. Fracture strength, hardness and chemical resistance tests were performed. A product with fine volumetric crystallization, a high degree of crystallization, having marble-like appearance, improved mechanical strength and suitable chemical durability was obtained. The material may be suitable for floor and wall tile applications in the construction industry.

1. Introduction

The manufacture of glass-ceramics offers a promising route for the commercial use of metallurgical slag. Such types of glass-ceramics can exhibit good fracture strength, chemical resistance and a highly attractive appearance that is suitable for application as wall and floor tiles. The removal of slag from the environment and the possibility of replacing natural stones, such as marble and granite, by glass-ceramic products, are highly appealing from the environmental standpoint and constitute a strongly motivating factor for research in this field.

Usiminas, a Brazilian steelmaker, produces approximately 100,000 t of blast furnace (BF) slag and 30,000 t of basic oxygen furnace (BOF) slag, per month. At present, the cement industry uses all the BF slag as raw material, but most of the BOF slag is still discarded. Some companies partially recover the scrap iron present in BOF slag, whose final residue can be either enriched with phosphorous and used as a fertilizer or used as crushed material for land leveling. However, part of this material still requires controlled disposal, and this need is the motivating factor in the search for engineering applications for BOF slag as an alternative raw material.

Received 18 June, revised manuscript 29 October 2001.

While the use of industrial and urban waste as raw materials for glasses and glass-ceramics has gained increasing importance in recent years [1 to 6], the literature still offers little information concerning the use of BOF slag for the same purpose. The use of BF slag for glass-ceramics is well known [7 to 9], but the analogous utilization of steel-making slag still constitutes a challenge. BOF slag possesses low concentrations of SiO_2 and a variable chemical composition, which hinders its use. Table 1 presents typical compositions of BF and BOF (BOF-1 and BOF-2) slag produced by Usiminas on different occasions.

Very few studies were focused on BOF slag. In the early 1980s, Kislitsyn et al. [10] successfully obtained a glass-ceramic using slag from an open-hearth furnace. This slag had a high iron concentration but its SiO_2 concentration was significantly higher than the modern BOF slag (see table 1). In the batch designed by those authors, the proportion of slag was about 60 wt%. Na_2O was added as sodium nitrate and soda. The experimental glasses were melted at 1450 to 1470 °C and volume crystallization occurred after treatment in the 800 to 1000 °C interval. Every glass tested showed some degree of internal crystallization, but required the addition of Cr_2O_3 to enhance nucleation and avoid deformation during its heat treatment. The physical properties of the resulting material were as good as those of a commercial BF-slag glass-ceramic.

Table 1. Slag glass compositions in wt%

component	BF	BOF-1	BOF-2	Kislitsyn [10]	Rabinovich [11]
SiO_2	33.3	13.7	10.3	31.9	15.8
Al_2O_3	12.7	1.1	3.9	3.9	5.2
Fe_2O_3	0.4	12.9	11.2	–	28.5
FeO	–	6.4	15.8	10.8	–
CaO	44.8	40.4	38.7	27.9	35.9
MgO	6.3	7.4	8.2	17.1	6.4
MnO	0.4	8.0	5.4	7.7	–
MnO_2	–	–	–	–	6.2
TiO_2	–	–	1.0	0.3	0.9
Na_2O	–	–	–	0.3	0.5
K_2O	–	–	–	0.1	–
Cr_2O_3	–	–	–	2.0	–
P_2O_5	–	2.0	1.7	–	–
SO_3	–	–	–	–	0.4
S^{2-}	–	–	0.2	0.2	–

Rabinovich [11] produced a glass-ceramic using a BOF slag (whose composition is shown in table 1). Glass-ceramics containing as much as 29 wt% Fe_2O_3 were developed. One of the glass compositions contained FeS as the nucleating agent. Apparently, manganese oxide also acted as a crystallization catalyst. The glasses were melted at 1550 to 1580 °C and poured into a metal mold to form (15 × 15 × 0.7) cm^3 plates. These thick plates were annealed in a crystallization furnace, previously heated to 500 to 550 °C, immediately after casting. The plates were crystallized by gradual heating to 1100 °C and soaked for 1 h at this temperature.

The main objective of this article is to explore the possibility of producing glasses and glass-ceramics using a BOF slag produced by Usiminas. Details concerning the melting, glass-forming ability and crystallization behavior of several slag-containing compositions are discussed. The mechanical and chemical properties of the developed glass-ceramics are evaluated and compared with those of similar commercial materials.

2. Experiments

2.1 Design and search for suitable glass compositions

Experimental compositions were prepared by mechanically mixing 50 to 75 wt% BOF-1 slag (see composition in table 1), and commercial-grade sand (with about 500 µm average particle size) in a set of batches. Sand was added to increase the SiO_2 concentration and improve the vitrificability of the melts. Its concentration in the batches was varied in an attempt to maximize the slag concentration, maintaining the glass-forming ability. The batches were heated to 1100 °C for 3 h, for pre-reaction and degassing, thereby preventing foaming. Mixtures of 100 g each were melted at 1450 °C for 1 h in $Al_2O_3-SiO_2-ZrO_2$ (ZAS) crucibles and splat-cooled between stainless steel plates to produce glass samples.

The sand was poorly assimilated into the melts. During melting, the undissolved sand remained adhered to the upper side of the crucible wall while the first liquid moved towards the bottom. Sodium carbonate was therefore added in new glass compositions to aid sand dissolution and avoid segregation.

New mixtures were prepared with finer (< 150 µm) sand, commercial-grade sodium carbonate and BOF-2 slag (see composition in table 1). The composition design followed an experiment-with-mixture approach [12] to optimize compositions for glass-ceramic production, taking into account the ease for melting and vitrification of the batch as well as its crystallization mechanism upon further heating.

Based on preliminary melting tests, we constrained the proportion of raw materials to the following limits: 40 to 80 wt% BOF-2 slag, > 10 wt% sand and 5 to 15 wt% Na_2O. The Na_2O concentration range (resulting after melting) was chosen to be equivalent to that in most common commercial glasses. The composition limits defined by the constraints form the polygon in the raw materials triaxial diagram shown in figure 1.

In figure 1, the compositions referring to the polygon vertices, the center of their longest edges and the center of their entire area form the set of eight experimental compositions taken for study. The proportion of raw materials in the designed mixtures, labeled 1 to 8, is given in table 2. A blend to produce 250 g of glass was prepared for each composition by mechanically mixing the raw materials, calcining the batch at 900 °C for 2 h and regrinding it to a powder. Mixtures of 125 g were melted at 1400 to 1450 °C for 1 h in Al_2O_3/ZrO_2 crucibles in a bottom-loaded electrical furnace. The mass to be melted was added to the crucible in doses of 25 g at a time to prevent foaming. After melting, the liquid was

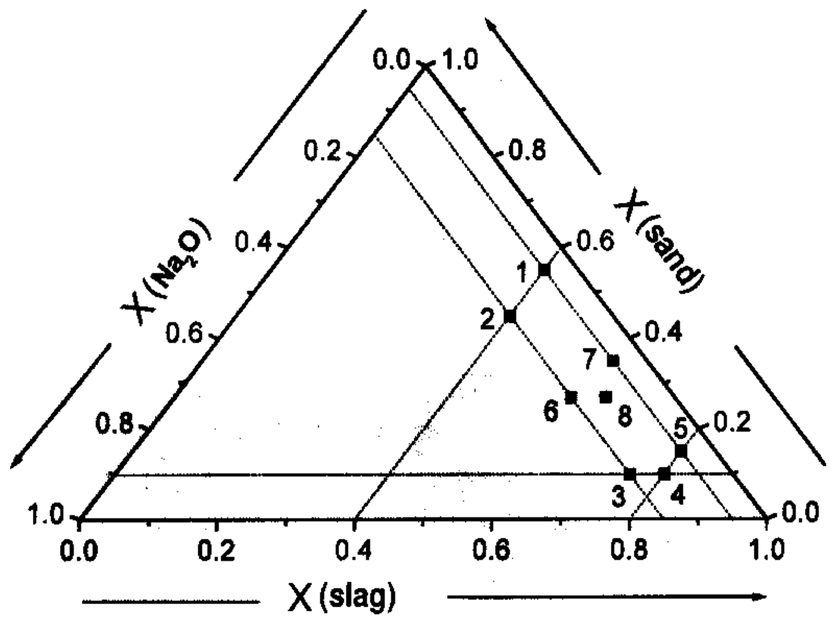

Figure 1. Constraints (-----) and designed sample compositions 1, 2, 3, 4, 5, 6, 7 and 8 (■) for the preparation of experimental slag glasses (X = mol fraction).

Table 2. Experimental slag glass compositions in wt%

sample	slag	sand	Na_2O
1	40	55	5
2	40	45	15
3	75	10	15
4	80	10	10
5	80	15	5
6	58	27	15
7	60	35	5
8	63	27	10

poured onto a stainless steel plate and splat-cooled. Each composition was prepared in duplicate and the samples were renamed SG-1A to 8A and SG-1B to 8B.

Differential scanning calorimetry (DSC) of samples with different grain sizes was used to study the crystallization behavior of compositions 1A to 8A, and was replicated in 1B to 8B. The samples were powdered in two particle size ranges: less than 74 µm and between 208 and 417 µm. The analyses were performed in a DSC model STA 409 (Netzsch-Gerätebau G.m.b.H., Selb (Germany)), on samples of approximately 20.0 mg, at a heating rate of 10 K/min and using Al_2O_3 as reference.

A systematic experimental study was carried out to identify the best conditions to produce a slag glass and the influence of these conditions on the crystallization kinetics. As will be justified later in this paper, composition 7 was chosen for further study and more glass of this composition was prepared.

A batch for 500 g of glass of composition 7 was melted at 1200 °C for 4 h in a ZAS crucible. This temperature was only a little above the liquidus temperature determined by DSC. The melt was poured and pressed between two stainless steel plates, forming thick (≈ 2 to 3 mm) glass plates that were ground and remelted to improve homogenization. The subsequent melting was carried out at 1200 °C for 4 h in a new ZAS crucible and cast into a graphite mold of (7 × 1 × 1) cm^3 to form samples denominated SG-7s1200. During this forming procedure, the melt partially solidified in the crucible owing to the temperature falling below liquidus. This solid was remelted by increasing the temperature to 1350 °C. The resulting liquid was cast into a stainless steel mold, forming a glass plate named SG-7s1350. The samples were annealed at 550 °C for at least 5 h.

In a new batch of composition 7, the melting temperature was raised to 1350 °C to prevent solidification during forming. A mixture for 300 g of glass was melted at 1350 °C for 1 h in ZAS crucibles. The liquid was poured into a stainless steel mold, allowed to cool, then ground and remelted. This procedure was repeated once more to improve homogenization. Finally, the batch was remelted at 1350 °C for 2 h. Part of the liquid was poured into graphite molds and the rest was splat-cooled. This glass, designated SG-7n, was annealed at 600 °C for 5 h and at 650 °C for 3 h.

In subsequent meltings for the production of samples for flexural and chemical resistance tests, a standard schedule was adopted based on the preceding experiments. For each new batch, a mixture to obtain 120 g of glass of composition 7 was melted in ZAS crucibles at 1350 °C for 4 h.

Homogenization was accomplished by vigorously shaking the crucible with tweezers several times during melting. After the holding time of 4 h, the melt was poured into graphite molds preheated to 500 °C to prevent thermal shock, producing bars of (7 × 1 × 1) cm^3. The samples were then immediately annealed at 580 °C for 3 h.

2.2 Nucleation kinetics determined by DSC

Many authors [13 to 18] have studied the possibility of obtaining crystal nucleation kinetics of glasses by thermal analysis (DTA or DSC), instead of directly counting the number of crystals in heat-treated samples. Ray and Day [18] showed that the plot of the inverse of the DSC crystallization peak temperature, ϑ_p^{-1}, of samples previously heat-treated in the nucleation range, as a function of the temperature of heat treatment, ϑ_n, resembles well the nucleation curve of the $Na_2O{\cdot}2CaO{\cdot}3SiO_2$ glass. However, that was not true when the peak height, $(\delta\vartheta)_p$, instead of the temperature, was used for the same task. That happens because the net shift of the crystallization peak temperature, caused by the heat treatment in the nucleation range, is proportional to the number of nuclei formed, while the shift in the peak height is also influenced by an overlapping crystal growth. The higher the number of nuclei for crystal growth, the larger will be the DSC peak shift to lower temperatures. Then, from $\vartheta_p^{-1} \times \vartheta_n$ plots it is possible to estimate the temperature were nucleation is maximum and also the temperature range where nucleation occurs.

The nucleation temperature range for glasses SG-7B, SG-7s1200 and SG-7n was estimated using DSC. The nucleation curve was obtained by measuring the crystallization peak temperature, ϑ_p, of samples previously heat-treated in the nucleation range – with a fixed time, heating rate, mass and grain size – and by plotting its inverse, ϑ_p^{-1}, against the temperature of the previous heat-treatment, ϑ_n. These analyses were performed in a DSC 404, Netzsch, and in a STA 409, Netzsch, using 30.0 mg samples with particle sizes ranging from 175 to 300 μm and at a heating rate of 20 K/min (before and after the isothermal heat treatments for nucleation). The isothermal heat treatments were carried out in the DSC furnaces, with a dwell time of 3 h. The analyses were made with the DSC reference crucible empty.

2.3 Thermal treatments

Crystallization treatments were done in a tubular electrical furnace. The temperature was measured within a precision of 1 K, using a thermocouple placed adjacent to the samples. There was no significant temperature gradient (< 2 K) in the furnace within a length of 10 cm, which sufficed to contain the samples. For the bending tests, the samples subjected to the same nucleation or growth schedule were heat-treated simultaneously.

2.4 Strength, hardness and chemical durability

Three-point bending strengths were measured using a universal testing instrument model 5500R (Instron Corp., Canton, MA (USA)), with 23.90 mm between load bearing supports and a crosshead speed of 0.5 mm/min [19]. The samples were prepared by cutting the original cast bars into smaller pieces (about $(0.5 \times 0.5 \times 3.5)$ cm^3, approximately half the length and width of the original bars), treating them for crystallization and grinding the surfaces with SiC 500 (average grain size of 18 μm and largest grain size of 35 μm) to produce plane parallel surfaces. Glass samples were also tested for comparison.

Vickers hardness, *HV*, was measured in a microhardness testing machine model FM-7e (Future-Tech Corp., Tokyo (Japan)), with a 100 g load and 5 s loading time. The load was calibrated using a metal standard (HV = (70 ± 0.2) GPa, at 100 g, under 5 s). Hardness was calculated as follows:

$$HV = \frac{1.854\,P}{d^2} \tag{1}$$

where P is the applied load and d is the diagonal length stamped on the sample's surface. Approximately 20 measurements were made for each material (glass and glass-ceramic).

Chemical resistance tests were performed by heating a sample with fixed mass and particle size in diluted acid or basic solutions and measuring the mass loss after the attack [1 and 20]. The composition-7 slag glass and glass-ceramic, a window glass, a natural white marble and a commercial gres-porcellanato tile were tested and the results compared. Powdered samples, with 300 to 500 μm particle diameter, each weighing 2 g, were heated at 95 °C for 1 h in 75-ml solutions 0.01 mol/l HCl or 0.01 mol/l NaOH. After the test, the material was washed in distilled water and acetone and oven-dried at 110 °C. The initial and final mass, m_0 and m_f, respectively, were measured using a 0.0001 g precision balance and the weight loss calculated as $m_p = (m_f - m_0)$. The resulting values were normalized by the specific surface, s_v, of each material, given by the equation (2)

$$s_v = \frac{6m_0}{D\varrho} \tag{2}$$

where D is the average particle diameter and ϱ is the mass density.

The mass density was measured in an Ultra Pycnometer 1000 (Quantachrome Corp., Syosset, NY (USA)).

The fractured sample surfaces that resulted from the three-point bending tests were observed in an SEM model XL 30 W/TMT (Philips Electron Optics, Eindhoven (Netherlands)). The samples were attacked for 10 s in 0.8 vol.% HCl and 0.2 vol.% HF solution to reveal their microstructure. X-ray diffraction (XRD) was carried out on powdered samples in an X-ray diffractometer model Geigelflex (Rigaku Denki Co. Ltd., Tokyo (Japan)) with an horizontal goniometer, Cu tube at 40 kV and 40 mA. The scan rate was 2°/min, in 0.02° steps from 5 to 100°.

3. Results and discussion

3.1 DSC results and choice of the SG-7 glass composition

The DSC results for the samples SG 1A to 8A were similar to their duplicate SG 1B to 8B. The curves for SG 1A to 8A, with different particle sizes, are shown in figure 2.

Compositions 1 to 8 presented different glass formation and crystallization behavior, observed during melting and forming and from the DSC results.

Compositions 3, 4 and 5 showed copious devitrification on cooling, during the casting and forming steps. Figure 2 (DSC traces for compositions 3 and 4) reveals the absence of crystallization, due to previous devitrification of the specimens. Nevertheless, the DSC traces of composition 5 showed small exothermic peaks, probably associated with the crystallization of a residual glass. The DSC behavior of composition 5 was surprisingly

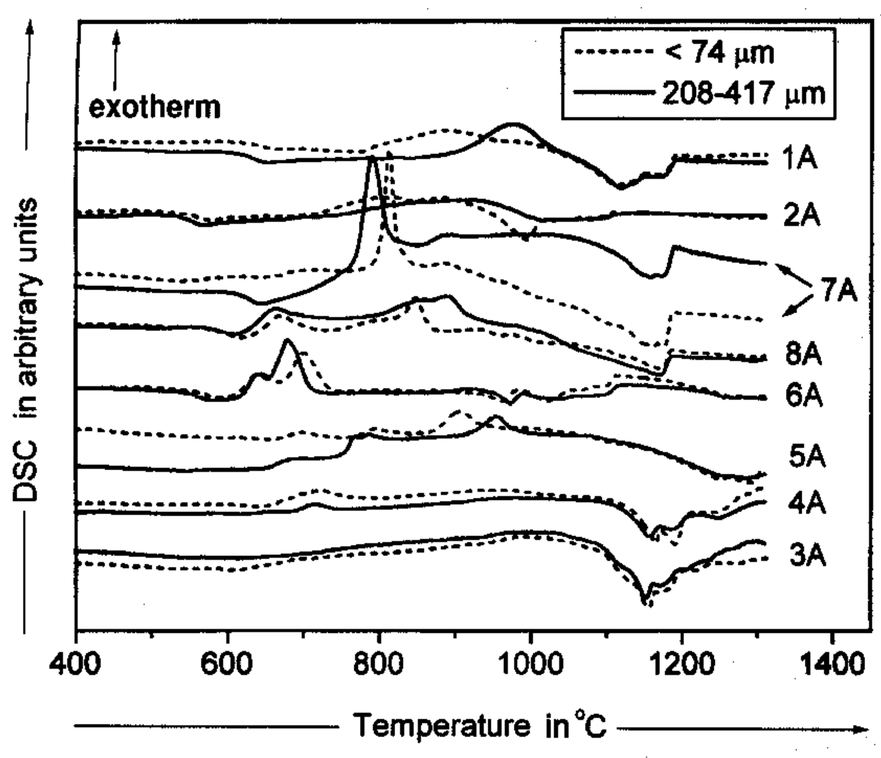

Figure 2. DSC curves for compositions SG-1 A to 8A; fine and coarse powders (heating rate= 10 K/min).

similar to that of composition 8, which contains a significantly higher amount of SiO_2. However, crystals from composition 5 presented higher crystallization and melting temperatures. All these compositions (except composition 8) showed an inferior glass-forming tendency and, thus, are of no practical interest.

Compositions 1 and 2 presented broad exothermic peaks in the crystallization range, typical of surface crystallization. Furthermore, the DSC crystallization peaks of the finer samples were clearly dislocated to lower temperatures, indicating that the finer the grain size and, hence, the higher the surface area, the more likely the crystallization. Only surface crystallization was observed in samples with composition 1, after different treatments at 700 °C for 1 h, at 750 °C for 1 h and at 885 °C for 30 min, and in a sample of composition 2 treated at 750 °C for 1 h. Trial tests to sinter glasses of these compositions were unsuccessful, since surface crystallization is much faster than viscous flow sintering.

Compositions 6 and 7 presented far more intense exothermic DSC peaks than the other glasses did. Moreover, the crystallization peaks of the coarse samples occurred at lower temperatures than those of the fine ones, suggesting bulk crystallization. An SEM analysis confirmed bulk crystallization in glasses of compositions 6 and 7 after thermal treatments in the crystallization range.

Compositions 5 and 8 showed a quite distinct behavior. Composition 5 readily devitrified during cooling, while composition 8 vitrified fairly easily. However, both compositions presented similar DSC behavior. Their DSC traces indicated the occurrence of initial bulk-like crystallization followed by surface-like crystallization in the same sample.

With the exception of compositions 5 and 8, the DSC results shown in figure 2, associated with direct observation during forming and after heat treatment, enabled us to classify the compositions into the categories shown in table 3.

Table 3. Classification of slag glass compositions as a function of devitrification behavior and crystallization mechanism (surface or bulk)

classification	sample
group 1: Reluctant glass formers (crystallize during forming)	3, 4
group 2: Intermediate glass formers (exhibit bulk crystallization after heat treatment)	6, 7
group 3: Good glass formers (exhibit only surface crystallization after heating)	1, 2

Composition 7 was chosen for further study because it displayed the most intense exothermic peak and (relatively) good glass-forming ability, indicating its tendency for fine interior crystallization. Its melt presents low viscosity and "short" behavior (large variation of viscosity within a small temperature change), which is then suitable for casting into molds. For the sake of simplicity, composition 7 will be labeled SG-7 and the respective glass-ceramic SGC-7.

3.2 SG-7 crystallization kinetics

It is difficult to determine the SG-7 nucleation kinetics by the traditional method [21 and 22]. In this method, crystal density in a transversal area across the sample is determined directly by microscopy as a function of the treatment temperature and time. A very high nucleation rate, leading to a great number of very fine crystals in the volume, hinders the practical determination of the SG-7 nucleation rates. Thus, we used DSC to indirectly measure the nucleation temperature range and the nucleation peak temperature.

Figure 3 shows the DSC curves obtained for SG-7B with different temperatures, ϑ_n, of previous (isothermal) heat treatments (see section 2.2), which reveal a (small) crystallization peak shift as a function of treatment temperature. The same procedure was adopted for SG-7s1200 (figure 4) and SG-7n (figure 5), which showed larger peak shift amplitudes.

Figures 3 to 5 do not always show the presence of only one exothermic peak, in the crystallization range, for a given treatment temperature. In some cases several peaks overlap, resulting in two maxima or a broader peak. At higher temperatures in the DSC curves, far from the first set of crystallization peaks, it is sometimes possible to detect a second (less intense) peak associated to a second phase (e.g., figure 4). Phase characterization will be presented later in this paper.

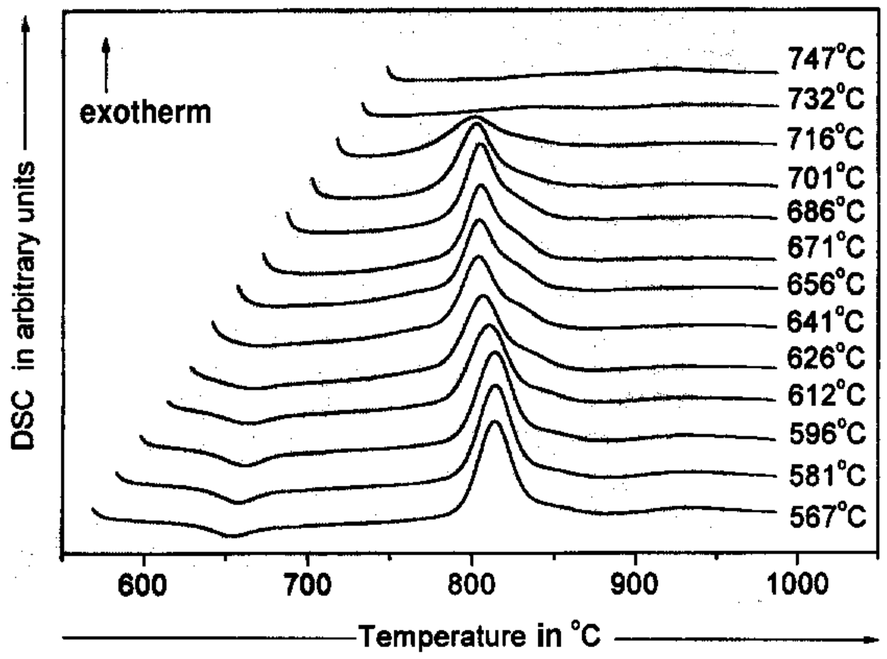

Figure 3. DSC curves for composition SG-7B treated for 3 h at different temperatures.

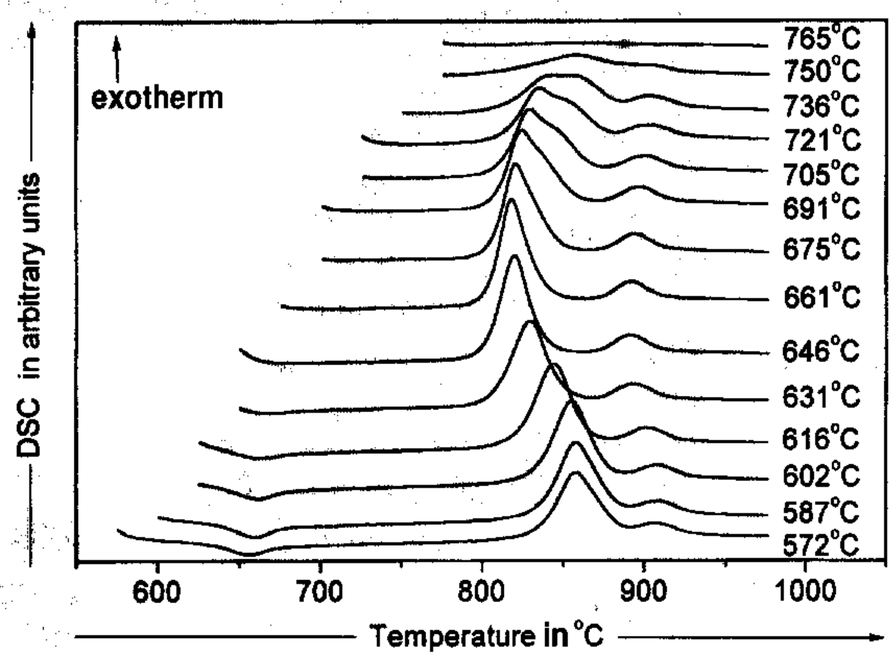

Figure 4. DSC curves for composition SG-7s1200 treated for 3 h at different temperatures.

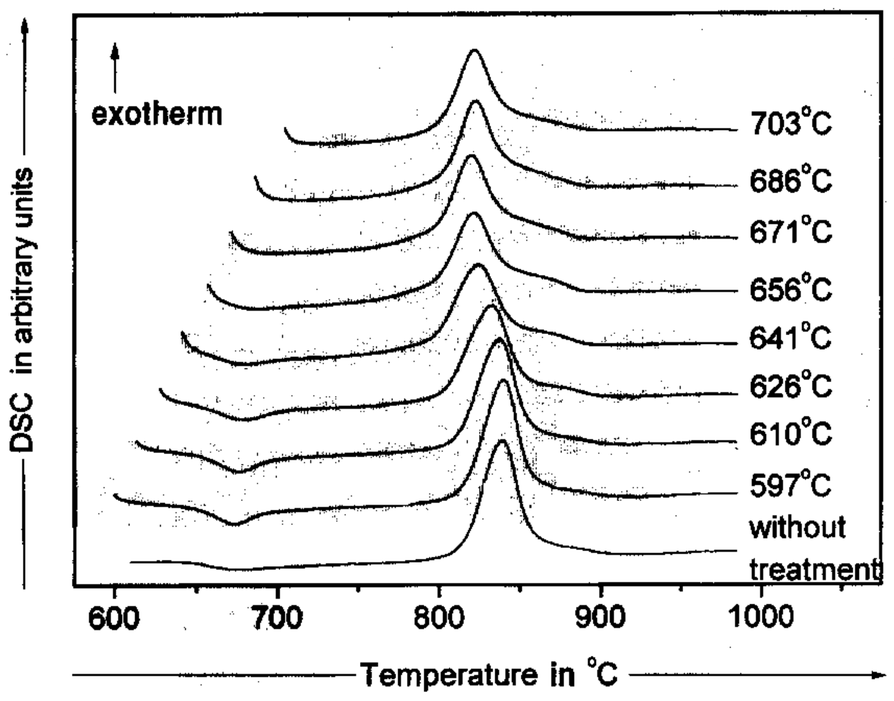

Figure 5. DSC curves for composition SG-7n treated for 3 h at different temperatures.

Figure 6 shows a plot of ϑ_p^{-1} as a function of ϑ_n, for each SG-7. The lowest-temperature (generally the most intense) DSC exothermic peak was taken in each case. For a comparison, the DSC peak magnitudes for the as-quenched glasses are shown as straight lines under the plots. The nucleation curves thus obtained present a

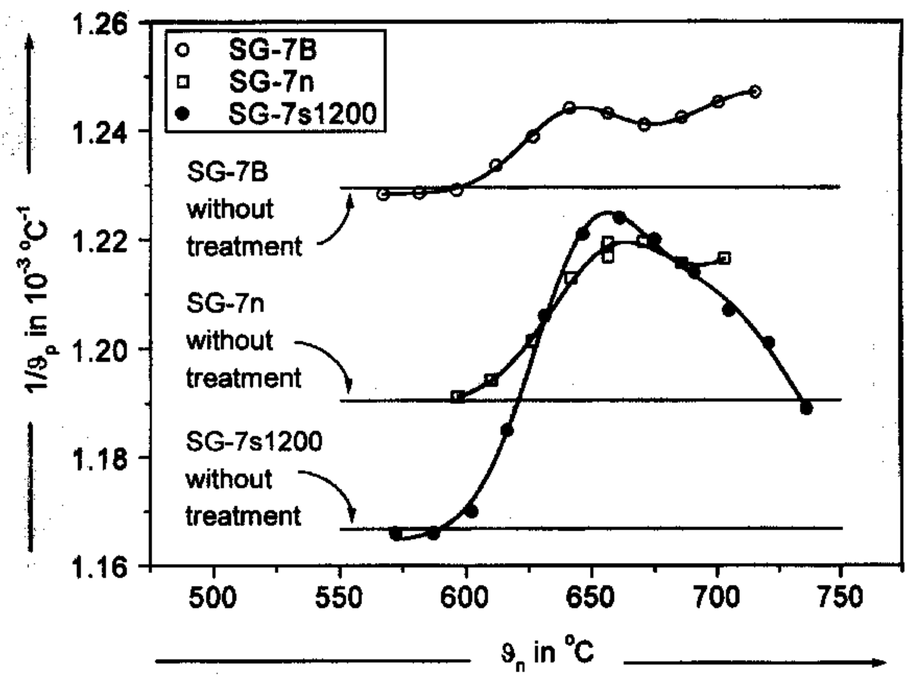

Figure 6. Nucleation curves for various SG-7 samples, with different preparation procedures. The straight lines under the plots correspond to the DSC peak magnitude for the as-quenched glasses. Curved lines are guides to the eyes.

maximum, ranging from approximately 647 °C for SG-7B to 664 °C for SG-7n. A maximum at 660 °C is also observed for SG-7s1200. For SG-7B and SG-7n, the maximum is less pronounced.

TEM micrographs and EDX results (not shown) show that internal crystals in the slag glass grow on iron-rich nuclei, probably a spinel-like magnetite, which often acts as a nucleation agent in similar systems [5 and 23]. This is clear evidence of heterogeneous nucleation and it will be the subject of a future paper. Then, the maximum in the curves of figure 6 cannot be attributed only to the nucleation kinetics in the slag glass, but mainly to the kinetics of spinel/magnetite precipitation and relates to the material's redox state, which changes according to preparation conditions.

In all the SG-7 compositions, the ϑ_p^{-1} for the as-quenched glasses, the presence of more than one exothermic peak in the crystallization range, and the amplitude of a peak shift as a function of previous heat-treatment temperatures presented differences from each other. The reasons for these differences were probably variations in raw material preparation, melting and cooling procedures and annealing conditions. Nevertheless, all the glasses apparently nucleate in similar temperature ranges.

In the ϑ_p^{-1} versus ϑ_n plot of figure 6, if one considers the range between the onset of the curve from the untreated-glass level and the corresponding maximum, one finds that nucleation ranged approximately between 580 and 660 °C. The peak in the DSC nucleation curves coincided for all glasses, lying at (657 ± 22) °C (95 % confidence limits), despite the melting differences. These values were then used to plan nucleation heat treatments.

DSC was also used to qualitatively estimate the isothermal crystal growth rate at different temperatures. The isothermal DSC traces of previously nucleated 40-mg monolithic SG-7 samples were registered during 1 h

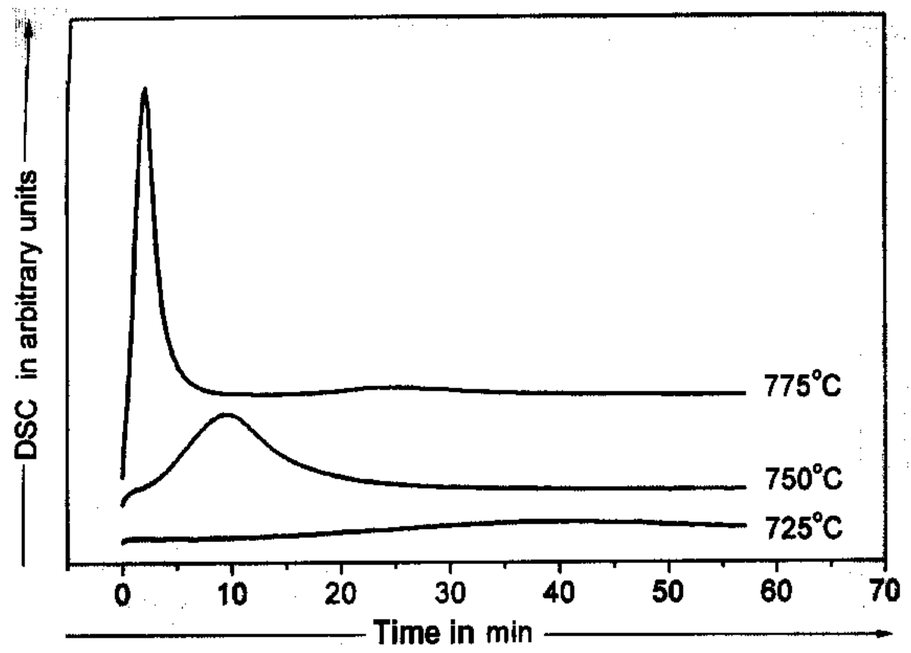

Figure 7. Isothermal DSC curves at different crystal growth temperatures of 40-mg SG 7 monolithic sample, pretreated at 666 °C for 3 h.

at the following temperatures: 725, 750 and 775 °C (figure 7). The samples were nucleated for 3 h at 660 °C in the DSC furnace, immediately before the isothermal DSC runs. The nucleation temperature was chosen according to the SG-7 nucleation maximum determined by DSC. The 3-h time period corresponds to that used to build the nucleation curves in figure 6. The heating rate (in the DSC) to reach the nucleation temperature and the rate between the nucleation and growth steps was fast (30 K/min) to minimize transformation during the ramp.

Figure 7 shows that, at 775 °C, there is a fast exothermic transformation in the first 5 to 10 min of treatment, followed by a second, much less intense transformation between 10 and 40 min. Qualitatively, figure 7 also shows that only the first crystallization peak is detected after 1 h at 750° and that, at 725 °C, this peak is incomplete in the 1-h treatment range.

XRD patterns of SG-7 treated at 662 °C for 3 h and at 775 °C for 5 min showed that a modified augite was the main phase crystallized. Alternatively, it is possible to suppose that two or more pyroxene solid solutions, near the augite composition, having subtle structural and chemical composition differences, are present at the same time. The XRD of SG-7 treated at 662 °C for 3 h and at 775 °C for 50 min showed the presence of wollastonite as a second phase.

3.3 Characterization and property measurements

The effect of a test heat treatment on the three-point bending strength of an SG-7 was preliminarily measured, before determining the nucleation range by DSC (figure 6). Four SG-7n test specimens were treated at 615 °C for 12 h and another four remained without treatment for comparison. The ground specimens were approximately 30 mm long, between 5.16 and 5.30 mm wide, and from 2.76 to 2.88 mm high.

The samples were accidentally mixed and, due to their similarity, it was unfortunately not possible to separate the results. However, as has been shown by figures 6 and 7, it was not expected that the treatment given sufficed to crystallize a significant volume fraction of the material at 615 °C, even after 12 h, since low nucleation and crystal growth rates are expected at this temperature.

As mentioned in section 2.1, the SG-7n had already been subjected to a previous annealing treatment at 650 °C for 3 h. The nucleation rate is already high in this temperature, as shown in figure 6, and site saturation is probably achieved after 3 h. However, as the material was not treated for crystal growth at higher temperatures, it was again expected that the transformed fraction represented only a small percentage of the material, which therefore remained mainly in glassy form. Thus, all the bending strength results were considered to be representative of the slag glass. Except for one highly discrepant result − 14 MPa − attributed to experimental error and therefore disregarded, the resulting seven-value average was (82 ± 8) MPa, within 95 % confidence limits. This value was taken as the representative SG-7 glass rupture strength.

Taking into account that the typical fracture toughness (K_{Ic}) for silicate glasses is between 0.7 and 0.9 MPa $m^{1/2}$, the size, c, of the surface flaw responsible for the fracture of our glasses can be estimated by equation (3) (considering that the flaw from which the crack propagated is much smaller than the sample thickness) [24], using the experimental fracture strength ($\bar{\sigma}$ = (82 ± 8) MPa)

$$c \cong \frac{1}{\pi}\left(\frac{K_{Ic}}{1.12\,\bar{\sigma}}\right)^2. \qquad (3)$$

The calculated flaw sizes range from 15 to 35 μm, which is in excellent agreement with the SiC-500 particle diameter (< 35 μm) used to grind the samples surface. We expect that the grinding procedure produced flaws on the glass surface with sizes similar to those calculated using equation (3). Hence, the glass fractures are obviously caused by cracks originating in the surface-grinding step.

New samples were prepared to evaluate the effect of nucleation and crystal growth on the mechanical properties. Crystallization treatments were carried out at two levels of temperature and time for nucleation and crystal growth, following a 4^2 factorial design [25], as shown in table 4. The nucleation temperatures were chosen within the nucleation range (figure 6), corresponding to a high and a low level within this range. The crystal growth temperatures were empirically found. Final specimen dimensions were around 30 mm long, 3.10 to 3.90 mm wide and 2.45 to 3.95 mm high.

The bending results are given in table 5, according to the treatment schedule shown in table 4. SEM micro-

Table 4. Variable levels of the 4^2 factorial design of the specimens' crystallization treatments for bending tests

variables	levels	
	low (−)	high (+)
nucleation temperature, ϑ_n, in °C	610	662
growth temperature, ϑ_c, in °C	700	750
nucleation time, t_n, in h	1	3
growth time, t_c, in h	1	3

graphs of fractured surfaces of all the tested samples are shown in figures 8a to d to 11a to d.

Based on the results of table 5 and on the microstructures of figures 8a to d to 11a to d (despite the fact that only one sample was tested under each set of conditions) it is possible to affirm that a high volume fraction of crystals improves the glass-ceramic fracture strength, regardless of the fact that some specimens had pores.

At growth temperatures below 700 °C, the nucleation time or temperature did not strongly influence the material's strength. At 700 °C, increased growth time from 1 to 3 h also caused no change. At this temperature, some treatments can produce a large number of internal crystals (e.g., figures 9c and d), but the crystals isolated in the glassy matrix did not influence the mechanical strength (that remained similar to that of the parent glass).

The effect of the nucleation temperature was increasingly significant with rising growth temperature, which exerted the strongest effect on the material's mechanical strength. Glass-ceramics produced at the highest growth temperature (750 °C) had the highest fracture strengths. Figures 10b to d and 11a to d clearly indicate that a high-crystallized volume fraction is responsible for the high mechanical strength achieved in these cases. However, as shown in the micrograph of figure 10a, a high growth temperature alone does not ensure a high-crystallized fraction if nucleation is not sufficiently intense. Also, even when a high strength is achieved, the low intensity of nucleation, resulting from either a low nucleation temperature or a short nucleation time or both, produces warped articles. Thus, an effective nucleation step is important to improve the mechanical strength and maintain the sample's dimensional integrity.

The increase in the mechanical strength of this glass-ceramic, therefore, probably depends mainly on its degree of crystallization. In other words, as long as a high-crystallized volume fraction is guaranteed, mechanical strength is apparently independent of grain size in the grain size range studied, because the surface flaw that causes fracturing is always much larger than the largest crystals in the glass-ceramic. The increased mechanical strength observed in the slag glass-ceramics with high-crystallized fraction is, thus, caused by an increase of K_{Ic}, which is typically observed for glass-ceramics.

The three-point bending results shown in table 5 can be divided into two classes: one for the glasses that reached full crystallization and increased mechanical strength, and the other for the glasses in which the residual glass fraction was too high, maintaining the material strength in the same order of magnitude as that of the glass. All the treatments covered in figures 8a to d, 9a to d, and 10a resulted in a high amount of residual glass and an average material strength of only (70 ± 8) MPa. This value matches that of the slag glass, (82 ± 8) MPa (within the limits of error). The treatments illustrated in figures 10b to d and 11a to d resulted in materials with high-crystallized fractions and an improved average three-point bending strength of (136 ± 14) MPa, which is approximately 50 % higher than the average strength of the parent glass.

Vickers microhardness was measured for an SG-7s1350 and for an SGC-7s1350 obtained by heat-treating the glass at 662 °C for 3 h and at 750 °C for 1 h. The results are shown in table 6. As long as the SG-7s1350 has a composition similar to that of other SG-7 and no important differences, except in melting parameters, no significant differences in properties are expected among them. The density of an SG-7 and an SGC-7 (obtained by the same crystallization schedule as SGC-7s1350) and their chemical resistance compared to those of commercial marble, window glass and gres-porcelanatto tiles are shown in table 6.

The properties of the slag glass-ceramic, table 6, are in good agreement with those of commercial materials,

Table 5. Three-point bending tests results; bending strength in MPa

treatment temperature in °C		treatment time in h			
		t_n = 1 (−)	3 (+)	1 (−)	3 (+)
ϑ_n	ϑ_c	t_c = 1 (−)	1 (−)	3 (+)	3 (+)
610 (−)	700 (−)	66	57	64*	63
662 (+)	700 (−)	64	76	71*	76
610 (−)	750 (+)	90*	123	114*	136*
662 (+)	750 (+)	128*	155	155*	140

* Warped samples.

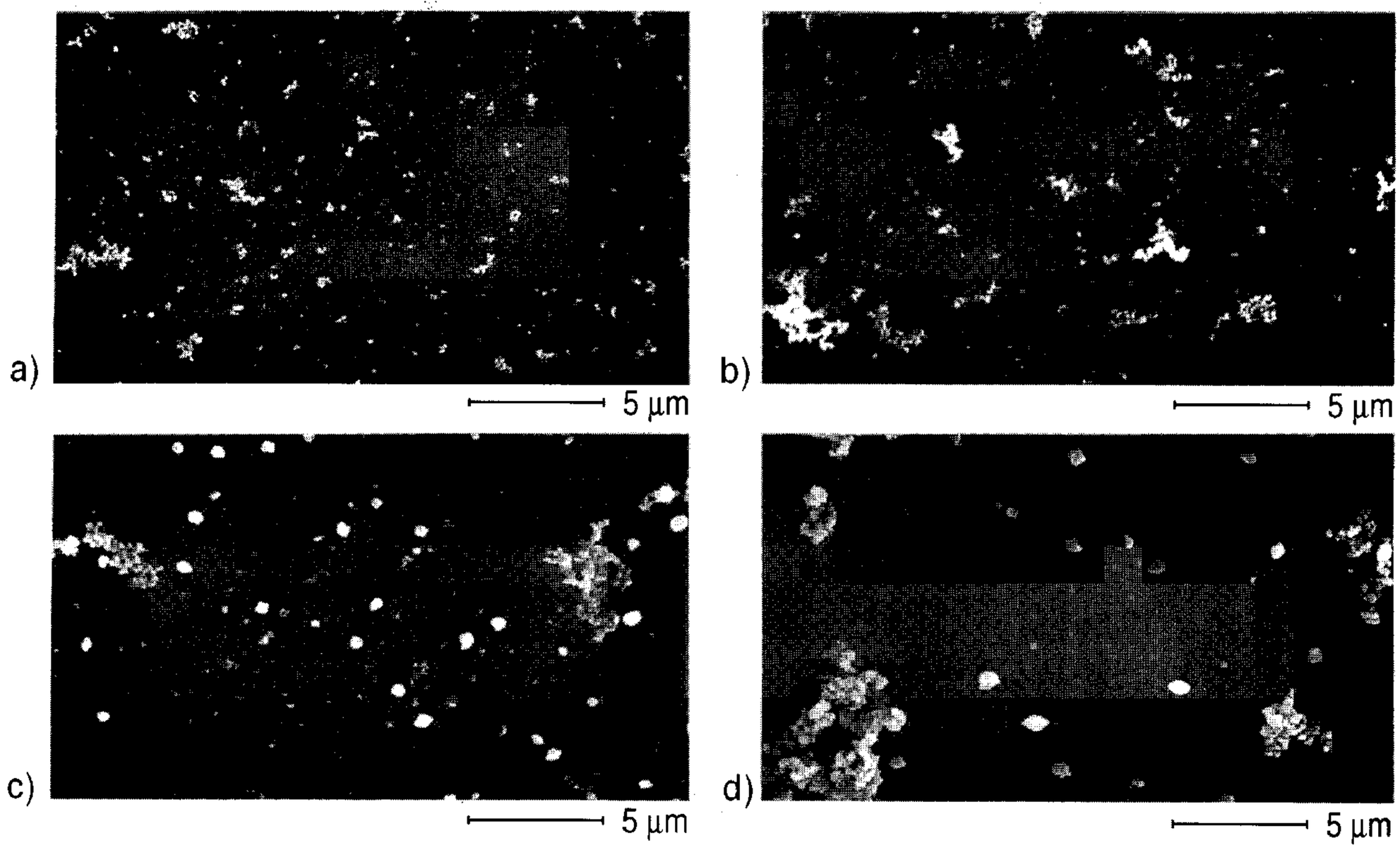

Figures 8a to d. SEM micrographs relative to values of table 5, first line (low ϑ_n and low ϑ_c):
a) ϑ_n (−), t_n (−), ϑ_c (−), t_c (−), 66 MPa;
b) ϑ_n (−), t_n (+), ϑ_c (−), t_c (−), 57 MPa;
c) ϑ_n (−), t_n (−), ϑ_c (−), t_c (+), 64 MPa;
d) ϑ_n (−), t_n (+), ϑ_c (−), t_c (+), 63 MPa.

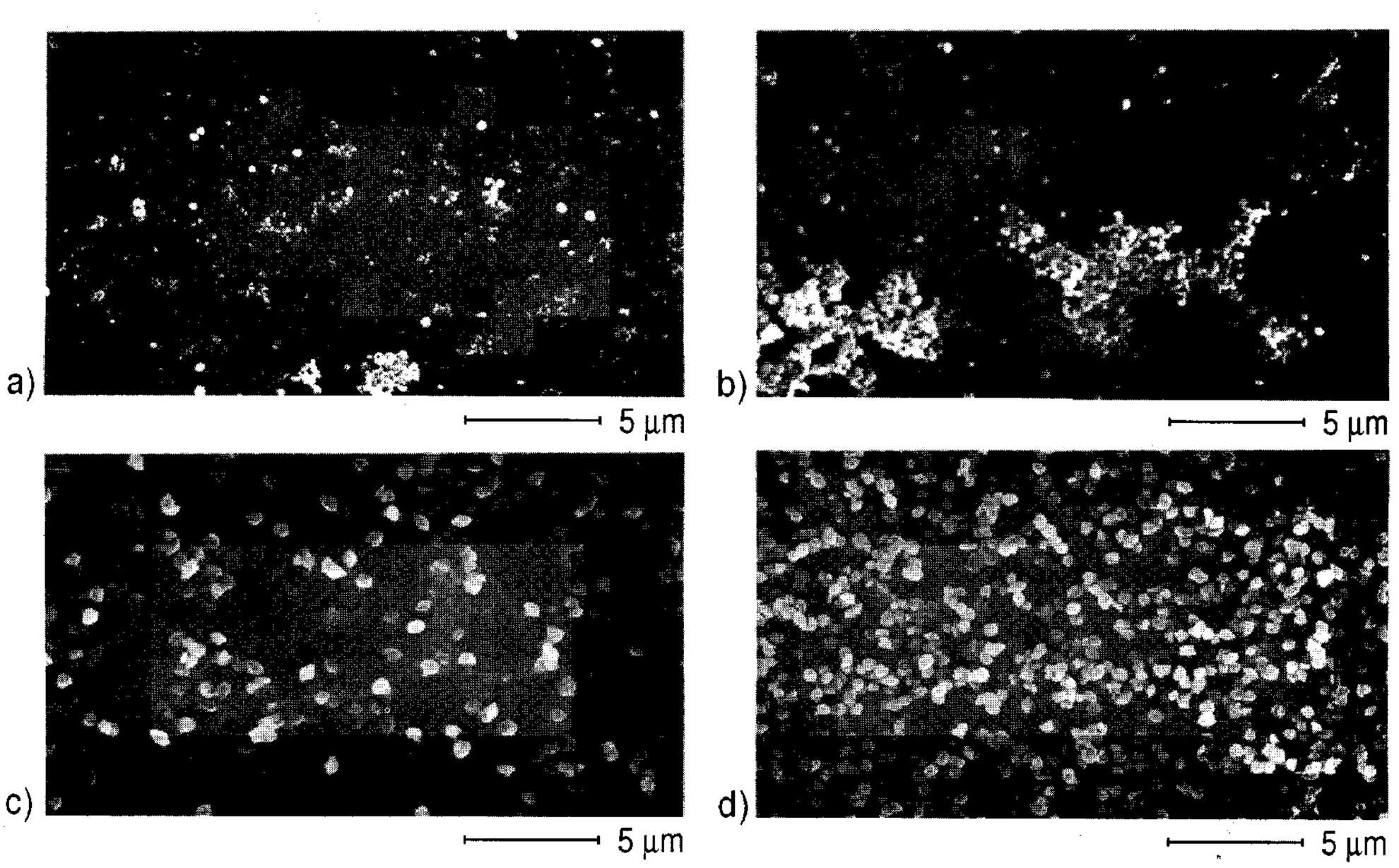

Figures 9a to d. SEM micrographs relative to values of table 5, second line (high ϑ_n and low ϑ_c):
a) ϑ_n (+), t_n (−), ϑ_c (−), t_c (−), 64 MPa;
b) ϑ_n (+), t_n (+), ϑ_c (−), t_c (−), 76 MPa;
c) ϑ_n (+), t_n (−), ϑ_c (−), t_c (+), 71 MPa;
d) ϑ_n (+), t_n (+), ϑ_c (−), t_c (+), 76 MPa.

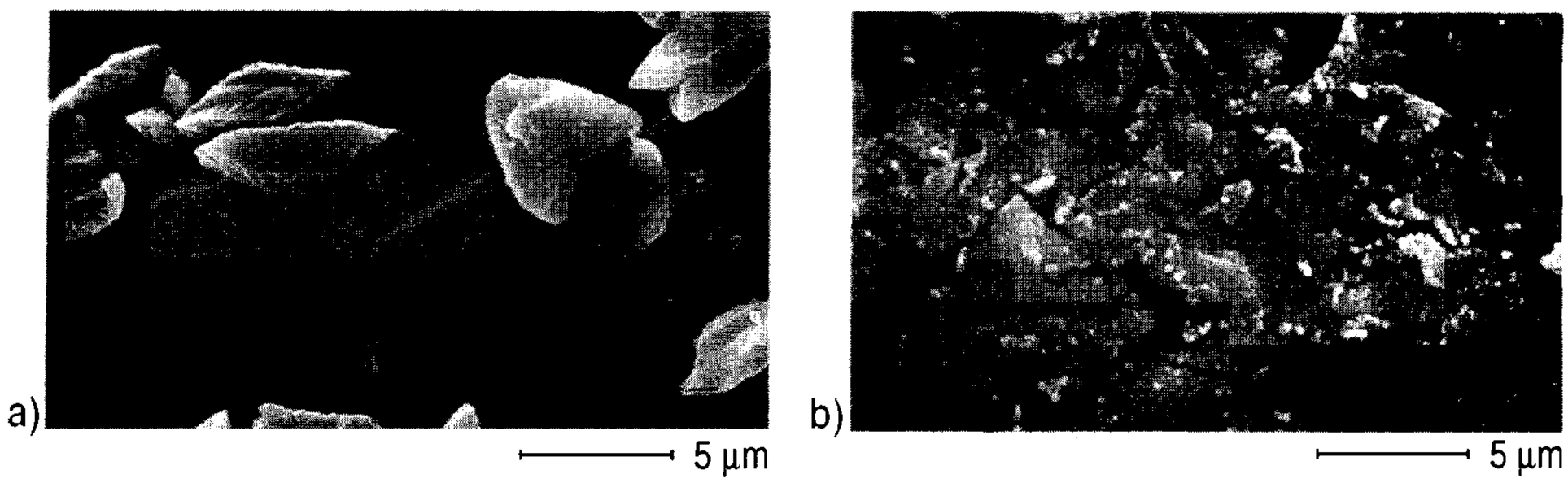

Figures 10a to d. SEM micrographs relative to values of table 5, third line (low ϑ_n and high ϑ_c):
a) ϑ_n (−), t_n (−), ϑ_c (+), t_c (−), 90 MPa;
b) ϑ_n (−), t_n (+), ϑ_c (+), t_c (−), 123 MPa;
c) ϑ_n (−), t_n (−), ϑ_c (+), t_c (+), 114 MPa;
d) ϑ_n (−), t_n (+), ϑ_c (+), t_c (+), 136 MPa.

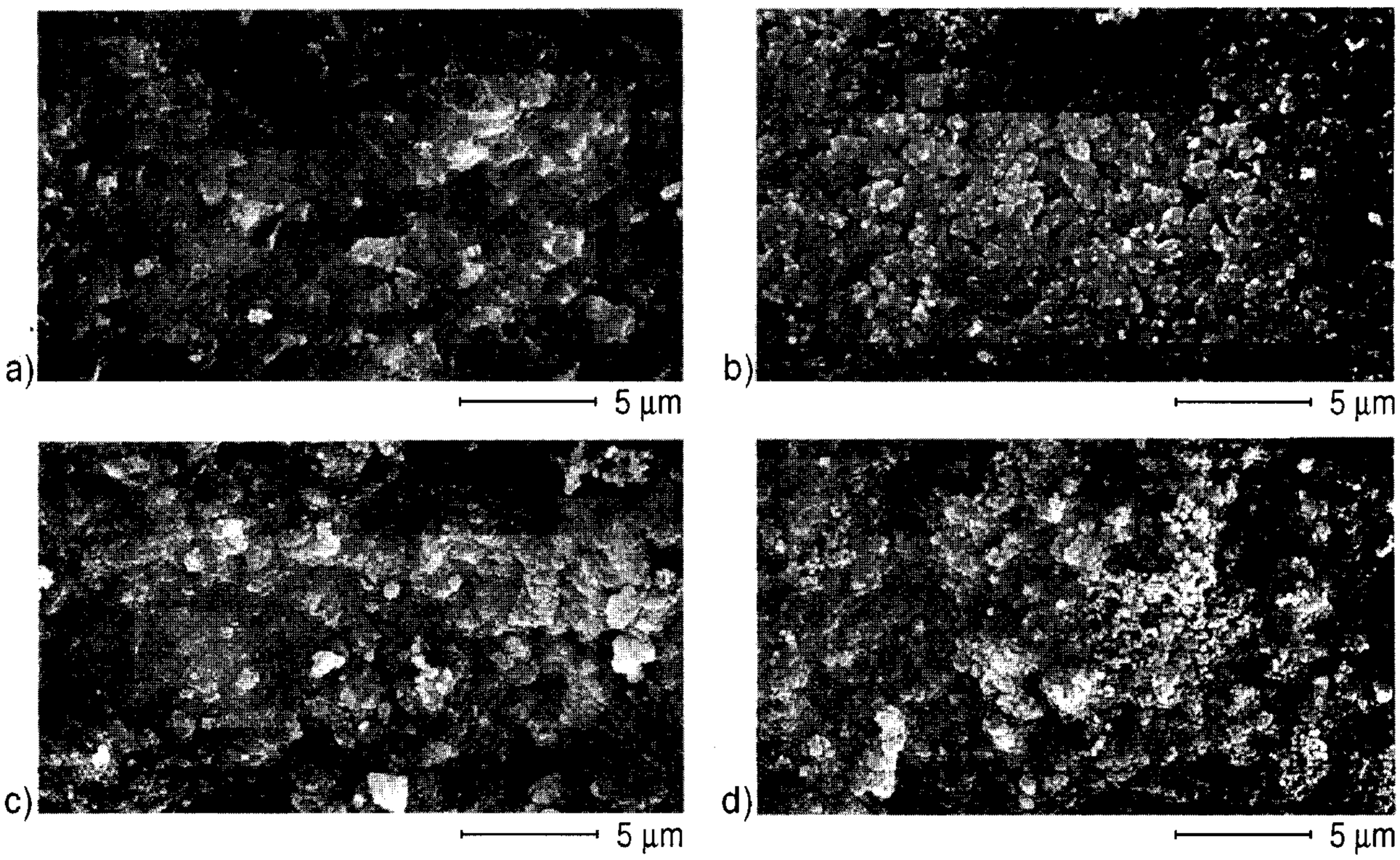

Figures 11a to d. SEM micrographs relative to values of table 5, fourth line (high ϑ_n and high ϑ_c):
a) ϑ_n (+), t_n (−), ϑ_c (+), t_c (−), 128 MPa;
b) ϑ_n (+), t_n (+), ϑ_c (−), t_c (−), 155 MPa;
c) ϑ_n (+), t_n (−), ϑ_c (+), t_c (+), 155 MPa;
d) ϑ_n (+), t_n (+), ϑ_c (+), t_c (+), 140 MPa.

Table 6. Properties of samples SG-7, SGC-7 and commercial materials

	SG-7	SGC-7	marble	soda-lime glass	gres-porcelanatto
three-point bending strength in MPa	70 ± 8	136 ± 14	5 ± 1	50 ± 20	–
density in g/cm^3	3.065 ± 0.001	3.300 ± 0.003	2.81	2.47 [26]	2.45
Vickers micro-hardness in GPa	6.9 ± 0.1	7.8 ± 0.2	0.03 ± 0.04	–	–
mass loss in acid solution in g	0.005 ± 0.001	0.019 ± 0.009	0.040 ± 0.005	0.002 ± 0.002	0.005 ± 0.008
mass loss in basic solution in g	0.001 ± 0.003	0.001 ± 0.002	0.002 ± 0.004	0.004 ± 0.006	0.0023 ± 0.0004

thus meeting several practical requirements. The material's visual appearance, as made or polished, is very attractive. With suitable optimization, it can be used in the form of floor or wall tiles in industrial, commercial and home construction applications [27].

4. Conclusions

With appropriate adjustments of its chemical composition and properly designed melting and thermal treatments, BOF slag can be used to produce glasses and glass-ceramics with good properties and a highly attractive appearance, suggesting that this material would be very suitable for applications such as construction tiles [27].

*

We acknowledge the funding provided by Usiminas and by the Brazilian agencies CAPES, CNPq and Pronex.

5. References

[1] Karamanov, A.; Gutzow, I.; Chomakov, I. et al.: Synthesis of wallcovering glass-ceramics from waste raw materials. Glastech. Ber. Glass Sci. Technol. **67** (1994) no. 8, p. 227–230.

[2] Romero, M.; Rincón, J. M.: Obtención y caracterización de vidrios obtenidos a partir de residues industriales de goethita (FeOOH). Bol. Soc. Esp. Ceram. Vidrio **36** (1997) no. 1, p. 39–45.

[3] Romero, M.; Rincón, J. M.: Surface and bulk crystallization of glass-ceramic in the Na_2O-CaO-ZnO-PbO-Fe_2O_3-Al_2O_3-SiO_2 system derived from a goethite waste. J. Am. Ceram. Soc. **82** (1999) no. 5, p. 1313–1317.

[4] Karamanov, A.; Cantalini, C.; Pelino, M. et al.: Kinetics of phase formation in jarosite glass-ceramic. J. Eur. Ceram. Soc. **19** (1999) p. 527–533.

[5] Karamanov, A.; Taglieri, G.; Pelino, M.: Iron-rich sintered glass-ceramic from industrial wastes. J. Am. Ceram. Soc. **82** (1999) no. 11, p. 3012–3016.

[6] Romero, M.; Rawlings, R. D.; Rincón, J. M.: Crystal nucleation and growth in glasses from inorganic wastes from urban incineration. J. Non-Cryst. Solids **271** (2000) p. 106–118.

[7] Hlavác, J.: The technology of glass and ceramics: an introduction. New York: Elsevier, 1983.

[8] Veasey, T. J.: Recent developments in the production of glass-ceramics. Miner. Sci. Engng. **5** (1973) no. 2, p. 92–107.

[9] Fredericci, C.; Zanotto, E. D.; Ziemath, E. C.: Crystallization mechanism and properties of a blast furnace slag glass. J. Non-Cryst. Sol. **273** (2000) p. 64–75.

[10] Kislitsyn, B. F.; Sas, R. I.; Golius, T. E. et al.: Synthesis of sitalls from open-hearth slag. Glass Ceram., NY, Consult. Bur. Transl. **38** (1981) no. 1–2, p. 13–14.

[11] Rabinovich, E. M.: Glass-ceramics from Israeli slag and coal ash. In: Simmons, J. H.; Uhlmann, D. R.; Beall, G. H. (eds.): Nucleation and crystallization in glasses. Columbus, OH: American Ceramic Society, 1982. p. 334–340.

[12] Cornell, J. A.: Experiments with mixtures – design, models and the analysis of mixture data. New York (et al.): Wiley, 1990.

[13] Marotta, A.; Buri, A.; Branda, F. et al.: Nucleation and crystallization of $Li_2O{\cdot}2SiO_2$ glass – a DTA study. In: Simmons, J. H.; Uhlmann, D. R.; Beall, G. H. (eds.): Nucleation and Crystallization in Glasses. Columbus, OH: American Ceramic Society, 1982. p. 146–152. (Advances in Ceramics. Vol. 4.)

[14] Ray, C. S.; Day, D. E.: Determining the nucleation rate curve for lithium disilicate glass by differential thermal analysis. J. Am. Ceram. Soc. **73** (1990) no. 2, p. 439–442.

[15] Xu, X. J.; Ray, C. S.; Day, D. E.: Nucleation and crystallization of $Na_2O{\cdot}2CaO{\cdot}3SiO_2$ glass by differential thermal analysis. J. Am. Ceram. Soc. **74** (1991) no. 5, p. 909–914.

[16] Weinberg, M. C.: Interpretation of DTA experiments used for crystal nucleation rate determinations. J. Am. Ceram. Soc. **74** (1991) no. 8, p. 1905–1909.

[17] Kelton, K. F.: Estimation of the nucleation rate by differential scanning calorimetry. J. Am. Ceram. Soc. **75** (1992) no. 9, p. 2449–2452.

[18] Ray, C. S.; Day, D. E.: An analysis of nucleation-rate type of curves in glass as determined by differential thermal analysis. J. Am. Ceram. Soc. **80** (1997) no. 12, p. 3100–3108.

[19] USA standard ASTM F417-78: Standard test method for flexural strength (modulus of rupture) of electronic-grade ceramics. In: Annual Book of ASTM Standards. Vol. 15.02, 1994.

[20] Karamanov, A.; Gutzow, I.; Penkov, I. et al.: Diopside marble-like sintered glass-ceramics. Glastech. Ber. Glass Sci. Technol. **67** (1994) no. 7, p. 202–206.

[21] James, P. F.: Kinetics of crystal nucleation in lithium silicate glasses. Phys. Chem. Glasses **15** (1974) no. 4, p. 95–105.

[22] Zanotto, E. D.; Galhardi, A.: Experimental test of the general theory of transformation kinetics: homogeneous nucleation in a $Na_2O{\cdot}2CaO{\cdot}3SiO_2$ glass. J. Non-Cryst. Solids **104** (1988) no. 1, p. 73–80.

[23] Rogers, P. S.; Williamson, J.: The nucleation of crystalline phases in silicate glasses containing iron oxides. Glass Technol. **10** (1969) no. 5, p. 128–133.

[24] Chiang, Y. M.; Birnie, D.; Kingery, W. D.: Physical ceramics – Principles for ceramic science and engineering. New York (et al.): Wiley, 1997.
[25] Box, G. E. P.; Hunter, W. G.; Hunter, J. S.: Statistics for experimenters – An introduction to design, data analysis, and model building. New York (et al.): Wiley, 1978.
[26] Navarro, J. M. F.: El Vidrio. Madrid: Consejo Superior de Investigaciones Cientificas, 1991.
[27] Ferreira, E. B.; Zanotto, E. D.; Fredericci, C. et al.: Black glass and dark glass-ceramic and method for making. (Orig. Port.) Brazilian pat. PI0005482 registered at INPI, Oct. 2000.

■ E202P003

Contact:

Eduardo B. Ferreira
DEMa/UFSCar
Rod. Washington Luis, km 235
13565-905 São Carlos, SP
(Brazil)
E-mail: pebf@iris.ufscar.br